## RESEARCH ARTICLE SUMMARY

## COSMOLOGY

# Constraints on the Hubble constant from supernova Refsdal's reappearance

Patrick L. Kelly\*, Steven Rodney, Tommaso Treu, Masamune Oguri, Wenlei Chen, Adi Zitrin, Simon Birrer, Vivien Bonvin, Luc Dessart, Jose M. Diego, Alexei V. Filippenko, Ryan J. Foley, Daniel Gilman, Jens Hjorth, Mathilde Jauzac, Kaisey Mandel, Martin Millon, Justin Pierel, Keren Sharon, Stephen Thorp, Liliya Williams, Tom Broadhurst, Alan Dressler, Or Graur, Saurabh Jha, Curtis McCully, Marc Postman, Kasper Borello Schmidt, Brad E. Tucker, Anja von der Linden

**INTRODUCTION:** The Hubble constant  $(H_0)$  quantifies the rate at which the Universe is expanding. It has been predicted that observations of a supernova (SN) that is multiply imaged by a foreground gravitational lens could, in principle, be used to measure  $H_0$ . The time delays between the SN's multiple images are expected to be inversely proportional to the value of  $H_0$ .

In late 2014, a SN was found that was strongly lensed by the galaxy cluster MACS J1149.5+2223. Dubbed SN Refsdal, it appeared in four images

around a galaxy that was a member of the cluster. Models of the gravitational lens predicted that a fifth image of SN Refsdal would appear within the next year. Multiple teams made blind predictions for the timing and relative brightness of the SN's reappearance.

**RATIONALE:** The two most precise previous measurements of the Hubble constant are inconsistent with each other (at  $>5\sigma$  significance), which is known as the Hubble tension. Measurements of thermonuclear supernovae (SNe)

B Sx
Spring 2016 imaging

Fall 2014 - spring 2015 imaging

SX
S2
S1
S3
S4

Appearance and reappearance of SN Refsdal, strongly lensed by the galaxy cluster MACS J1149.5+2223. Both panels were taken with the Hubble Space Telescope. (A) Images S1 to S4 (labeled) of SN Refsdal appear in an Einstein cross configuration in 2014. Models predicted the appearance of an additional image SX in the region denoted by the red box. (B) Observation of SX in spring 2016 after its appearance in late 2015. In (A), colors were assigned to coadded images taken in these filters: blue, F606W (V-band) and F814W (I-band); green, F105W (Y-band) and F125W (J-band); and red, F140W (between the J- and H-bands) and F160W (H-band). The image in (B) used only the F125W filter, so it is shown in grayscale.

in the nearby Universe have yielded  $H_0=73$  1.0 km s<sup>-1</sup> Mpc<sup>-1</sup>. Observations of the cosmicrowave background (CMB) have led to a lower value of  $H_0=67.4\pm0.6$  km s<sup>-1</sup> Mpc<sup>-1</sup>, assuming standard cosmology. If this tension is confirmed using independent measurements, it could indicate problems with standard cosmology. An alternative cosmology, such as those involving an additional early dark energy or more species of particles, might be required to reconcile the measurements.

The predicted additional image of SN Refsdal appeared in 2015. Follow-up observations have allowed the time delays and magnification ratios between the multiple images to be determined. We combine those measurements with the pre-reappearance model predictions to perform a blinded calculation of the value of  $H_0$ .

**RESULTS:** We compute the likelihood of the time delay, magnification, and position measurements given each lens model's predictions after rescaling the time delay predictions for different values of  $H_0$ . This approach weights each model's contributions in a combined constraint on  $H_0$ . Weights are assigned according to each model's ability to reproduce the observations that are independent of  $H_0$  (location of the reappearance, magnification ratios, and ratios of time delays).

We perform two estimates of  $H_0$ : (i) from all lens models that made published predictions before the reappearance was observed and (ii) using a subset of those models, by selecting those that are most consistent with the observations and dominate the weights.

**CONCLUSION:** We infer a value of  $H_0$  of  $64.8^{+4.4}_{-4.3}$  km s<sup>-1</sup> Mpc<sup>-1</sup> using the full set of eight prereappearance models and of  $66.6^{+4.1}_{-3.3}$  km s<sup>-1</sup> Mpc<sup>-1</sup> from the two preferred models. Our results are most consistent with the  $H_0$  value measured from the CMB but do not exclude the higher value from nearby SNe.

We used a simulation of a galaxy cluster lens to verify that the uncertainty on our measurement of  $H_0$  is consistent with expectations. The ability of the lens models to reproduce the positions of the SN images also implies an expected uncertainty on  $H_0$ , which we find agrees with our constraints. The best agreement between lens models and observations that are independent of  $H_0$  is achieved by the models that were constructed by assigning dark-matter halos to both the cluster and to individual galaxies in the cluster.  $\blacksquare$ 

The list of author affiliations is available in the full article online. \*Corresponding author. Email: plkelly@umn.edu
Cite this article as P. L. Kelly et al., Science 380, eabh1322
(2023). DOI: 10.1126/science.abh1322



## **READ THE FULL ARTICLE AT**

https://doi.org/10.1126/science.abh1322

## RESEARCH ARTICLE

## COSMOLOGY

# Constraints on the Hubble constant from supernova Refsdal's reappearance

Patrick L. Kelly<sup>1\*</sup>, Steven Rodney<sup>2</sup>, Tommaso Treu<sup>3</sup>, Masamune Oguri<sup>4,5,6</sup>, Wenlei Chen<sup>1</sup>, Adi Zitrin<sup>7</sup>, Simon Birrer<sup>8,9</sup>, Vivien Bonvin<sup>10</sup>, Luc Dessart<sup>11</sup>, Jose M. Diego<sup>12</sup>, Alexei V. Filippenko<sup>13,14</sup>, Ryan J. Foley<sup>15</sup>, Daniel Gilman<sup>16,3</sup>, Jens Hjorth<sup>17</sup>, Mathilde Jauzac<sup>18,19,20,21</sup>, Kaisey Mandel<sup>22,23</sup>, Martin Millon<sup>10,8</sup>, Justin Pierel<sup>24,2</sup>, Keren Sharon<sup>25</sup>, Stephen Thorp<sup>26,22</sup>, Liliya Williams<sup>1</sup>, Tom Broadhurst<sup>27</sup>, Alan Dressler<sup>28</sup>, Or Graur<sup>29,30</sup>, Saurabh Jha<sup>31</sup>, Curtis McCully<sup>32,33</sup>, Marc Postman<sup>24</sup>, Kasper Borello Schmidt<sup>34</sup>, Brad E. Tucker<sup>35,36,37</sup>, Ania von der Linden<sup>9</sup>

The gravitationally lensed supernova Refsdal appeared in multiple images produced through gravitational lensing by a massive foreground galaxy cluster. After the supernova appeared in 2014, lens models of the galaxy cluster predicted that an additional image of the supernova would appear in 2015, which was subsequently observed. We use the time delays between the images to perform a blinded measurement of the expansion rate of the Universe, quantified by the Hubble constant ( $H_0$ ). Using eight cluster lens models, we infer  $H_0 = 64.8^{+4.4}_{-3.3}$  kilometers per second per megaparsec. Using the two models most consistent with the observations, we find  $H_0 = 66.6^{+4.1}_{-3.3}$  kilometers per second per megaparsec. The observations are best reproduced by models that assign dark-matter halos to individual galaxies and the overall cluster.

trong gravitational lensing occurs when the gravitational influence of a foreground mass, such as a galaxy cluster, produces multiple images of a well-aligned background source. In principle, the time delays between the images of a strongly lensed supernova (SN) directly determine the geometric distance, which enables a measurement of the Hubble constant  $H_0$  (1). Although originally proposed for supernovae (SNe), this technique, known as time-delay cosmography (2), has only been applied to quasars strongly lensed by single-galaxy foreground lenses (3-5). The strongly lensed SN Refsdal appeared in late 2014 in four resolved images, designated S1 to S4 (coordinates listed in table S1), arranged in a cross-like configuration (known as an Einstein cross) around an early-type member of the galaxy cluster MACS

J1149.5+2223 (right ascension 11h49m35.8s, declination +22°23′55″, all coordinates are J2000 equinox; hereafter referred to as MACS J1149) (fig. S1A) (6). Models of the gravitational lens predicted that an additional image would appear, designated SX (table S1), which was observed in 2015 (fig. S1B) (7). A companion paper (8) has measured the relative time delay between the images S1 to S4 and image SX as  $376.0_{-5.5}^{+5.6}$  days, a precision of 1.5%, using Hubble Space Telescope (HST) observations in the nearinfrared F125W (J-band) and F160W (H-band) broadband filters. If the matter distribution in the foreground MACS J1149 cluster lens were known exactly, time-delay cosmography could provide a measurement of  $H_0$  with equivalent 1.5% precision.

The value of  $H_0$  is currently debated because of a tension between early-time and late-time

probes of the expansion rate of the Universe. Assuming a standard cosmological model with flat geometry, a cosmological constant  $\Lambda$ , and cold dark matter (CDM), the cosmic microwave background (CMB) measurements using the *Planck* satellite imply  $H_0=67.4\pm0.6\,\mathrm{km\,s^{-1}\,Mpc^{-1}}$  (9). By contrast, the alternative local distance ladder method, used by the Supernova H0 for the Equation of State (SH0ES) team, yields  $H_0=73.04\pm1.04\,\mathrm{km\,s^{-1}}$  Mpc<sup>-1</sup> (10). This tension between the SH0ES and *Planck*  $H_0$  measurements has >5 $\sigma$  statistical significance, indicating a potential problem with standard cosmology (11).

Measurements of  $H_0$  using independent techniques are needed to confirm or refute the apparent tension. A local distance ladder measurement using the tip of the red giant branch (TRGB) method yields  $H_0 = 69.8 \pm$  $0.8(stat) \pm 1.7(sys) \text{ km s}^{-1} \text{ Mpc}^{-1}$  (12). Timedelay cosmography using quasar systems, multiply imaged by foreground galaxy-scale lenses, find  $H_0 = 73.7^{+1.4}_{-1.5} \, \mathrm{km \, s^{-1} \, Mpc^{-1}}$  (13) or  $H_0 = 74.5^{+5.6}_{-6.1} \, \mathrm{km \, s^{-1} \, Mpc^{-1}}$  (with broader assumptions) for time-delay lenses and  $H_0 = 68.4^{+4.1}_{-3.2} \, \mathrm{km \, s^{-1} \, Mpc^{-1}}$  when combining timedelay lenses with non-time-delay lenses at lower redshift, assuming that both are drawn from the same parent population (14). The appearance of the final image of SN Refsdal provides an opportunity to make an independent measurement of  $H_0$  using models of MAC J1149 (15, 16). The systematic uncertainties of cluster-scale models (17) differ from the galaxy-scale models used for quasar timedelay measurements.

Lensed SNe (18) are predicted to provide more precise time-delay measurements than quasar observations and require shorter observations spanning months or years (19–21). Time delays of months or years are expected to be unusual among SNe that are strongly lensed by clusters with extensive preexisting observations (22). The massive galaxy cluster MACS J1149 [total mass  $(1.4 \pm 0.3) \times 10^{15} \,\mathrm{M}_{\odot}$  (23–25)] was observed numerous times before

1 Minnesota Institute for Astrophysics, University of Minnesota, Minneapolis, MN 55455, USA, 2 Department of Physics and Astronomy, University of South Carolina, Columbia, SC 29208, USA, <sup>3</sup>Department of Physics and Astronomy, University of California, Los Angeles, CA 90095, USA. <sup>4</sup>Center for Frontier Science, Chiba Úniversity, Chiba 263-8522, Japan. <sup>5</sup>Research Center for the Early Universe, University of Tokyo, Tokyo 113-0033, Japan. 6 Kavli Institute for the Physics and Mathematics of the Universe, University of Tokyo, Kashiwa, Chiba 277-8583, Japan. 7 Physics Department, Ben-Gurion University of the Negev, Beer-Sheva 8410501, Israel. 8Kavli Institute for Particle Astrophysics and Cosmology, Stanford University, Stanford, CA 94305, USA. 9Department of Physics and Astronomy, Stony Brook University, Stony Brook, NY 11794, USA. 10Laboratoire d'Astrophysique, Ecole Polytechnique Federale de Lausanne, Observatoire de Sauverny, CH-1290 Versoix, Switzerland. 11 Institut d'Astrophysique de Paris, Centre National de la Recherche Scientifique-Sorbonne Université, F-75014 Paris, France. 12 Instituto de Física de Cantabria, Consejo Superior de Investigaciones Científicas y la Universidad de Cantabria, 39005 Santander, Spain. 13 Department of Astronomy, University of California, Berkeley, CA 94720, USA. <sup>14</sup>Miller Institute for Basic Research in Science, University of California, Berkeley, CA 94720, USA. <sup>15</sup>Department of Astronomy and Astrophysics, University of California Observatories, Lick Observatory, University of California, Santa Cruz, CA 95064, USA. <sup>16</sup>Department of Astronomy and Astrophysics, University of Toronto, ON, M5S 3H4, Canada. <sup>17</sup>Dark Cosmology Centre, Niels Bohr Institute, University of Copenhagen, DK-2100 Copenhagen, Department of Physics, Durham DH1 3LE, UK. <sup>19</sup>Institute for Computational Cosmology, Durham University, Durham DH1 3LE, UK. <sup>20</sup>Astrophysics Research Center, University of KwaZulu-Natal, Durban 4041, South Africa. <sup>21</sup>School of Mathematics, Statistics, and Computer Science, University of KwaZulu-Natal, Durban 4041, South Africa. 22 Institute of Astronomy and Kavli Institute for Cosmology, Cambridge CB3 OHA, UK. <sup>23</sup>Statistical Laboratory, Department of Pure Mathematics and Mathematical Statistics, University of Cambridge, Cambridge CB3 OWB, UK. <sup>24</sup>Space Telescope Science Institute, Baltimore, MD 21218, USA. <sup>25</sup>Department of Astronomy, University of Michigan, Ann Arbor, MI 48109, USA. <sup>26</sup>The Oskar Klein Centre, Department of Physics, Stockholm University, AlbaNova, 10691
Stockholm, Sweden. <sup>27</sup>Ikerbasque Foundation, University of the Basque Country, Donosita International Physics Center, Donostia, Spain. <sup>28</sup>The Observatories of the Carnegie Institution for Science, Pasadena, CA 91101, USA. <sup>29</sup>Institute of Cosmology and Gravitation, University of Portsmouth, Portsmouth PO1 3FX, UK. <sup>30</sup>Department of Astrophysics, American Museum of Natural History, New York, NY 10024, USA. <sup>31</sup>Lepartment of Physics and Astronomy, Rutgers, The State University of New Jersey, Piscataway, NJ 08854, USA. <sup>32</sup>Las Cumbres Observatory, Goleta, CA 93117, USA <sup>33</sup>Department of Physics, University of California, Santa Barbara, CA 93106, USA <sup>34</sup>Leibniz-Institut fur Astrophysik Potsdam, 14482 Potsdam, Germany, <sup>35</sup>The Research School of Astronomy and Astrophysics, Mount Stromlo Observatory, Australian National University, Canberra, ACT 2611, Australia. <sup>36</sup>National Centre for the Public Awareness of Science, Australian National Úniversity, Canberra, ACT 2611, Australia. 37The Australian Research Council Centre of Excellence for All-Sky Astrophysics in 3 Dimensions, ACT 2611, Australia. \*Corresponding author. Email: plkelly@umn.edu

the appearance of SN Refsdal, placing strong constraints on its mass distribution (26-28). Numerous teams have used lens models to predict the reappearance of SN Refsdal, before the observation of SX (29,30). These models used several different assumptions, so the appearance of SX can also be used to test those assumptions.

The reappearance of SN Refsdal, in image SX, was detected in HST observations taken on 11 December 2015 universal time (UT) (6) and was reported to the community the next day (31). This initial observation was used to estimate the relative time delay between SX and S1 as 320 to 380 days (32).

Each lens model yielded predictions  $\Delta t_{\rm X,1}^{\rm pred,70}$  for the relative time delay between images SX and S1 (designated by the subscripts X and 1, respectively) as well as between other image pairs, assuming  $H_0=70~{\rm km~s^{-1}~Mpc^{-1}}$  (denoted by the superscript 70). For fixed values of the cosmological matter density parameter  $\Omega_M$  and the dark energy density  $\Omega_\Lambda$ , the predicted time delay  $\Delta t_{\rm X,1}^{\rm pred}(H_0)$  for a given value of  $H_0$  depends inversely on the value of  $H_0$ 

$$\Delta t_{\mathrm{X},1}^{\mathrm{pred}}(H_0) = \Delta t_{\mathrm{X},1}^{\mathrm{pred},70} \times \frac{70 \,\mathrm{km \, s^{-1} \, Mpc^{-1}}}{H_0}$$
(1)

which allows the predicted time delay to be computed for a given value of  $H_0$  for each model. The uncertainty associated with this rescaling of the predictions is smaller than  $\sim 0.7 \text{ km s}^{-1} \text{ Mpc}^{-1}$ , given the weak dependence of  $H_0$  on  $\Omega_M$  and  $\Omega_\Lambda$ . Using a simulation of a galaxy cluster (33), we calculate that the single model that receives the greatest weight in our analysis can recover  $H_0$  with at least 5% accuracy (34). We also determine that our error budget is consistent with the model's astrometric errors (35).

We use two sets of lens models to compute parallel estimates of the value of  $H_0$ , using our observations of SN Refsdal. We first obtain an estimate of the value of  $H_0$  using a set of predictions from eight models—which we refer to as the Diego-a free-form model (29); the Zitrin-c\* light-traces-mass (LTM) model (29); and the Grillo-g (29), Oguri-a\* and Oguri-g\* (29), Jauzac-15.2\* (30), and Sharon-a\* and Sharon-g\* (29) simply parameterized models. Models that are simply parameterized use easy-to-compute parametric forms to describe the distribution of dark matter, using priors inferred from the luminous tracers and cosmological simulations. They include one or more cluster-scale halos and assign a darkmatter halo to each luminous galaxy-cluster member after scaling the halo mass according to the galaxies' properties, such as stellar mass or velocity dispersion. The second, parallel estimate includes only the Grillo-g and Oguri-a\* models, which we selected before unblinding the time delay, as explained below. In both cases, each model's contribution to the  $H_0$  inference is weighted according to its ability to reproduce  $H_0$ -independent observables.

## **Blinded analysis**

To avoid human bias, we carried out our analysis without knowledge of the time-delay measurements and the implied value of  $H_0$ . For the light curve (flux as a function of time) of each of the images S1 to SX, we selected a random number, whose value was stored but kept hidden, which was added to the dates associated with the flux measurements, shifting the light curve in time by an unknown amount (8). Before unblinding the time delay, we were only aware that the relative delay of SX and S1 was in the range of 320 to 380 days (68% confidence level) from a previously published analysis of two epochs of imaging (36). This range corresponds to ~17% in  $H_0$  before unblinding.

## Observables used for likelihood functions

We use constraints on the time delay between images A and B from the observed light curves (LCs) expressed as a probability  $P(\Delta t_{\rm A,B}|{\rm LC})$ . The prediction for the time delay,  $\Delta t_{\rm A,B}^{\rm pred,70}$ , from each lens model  $M_l$  is then used with Bayes' theorem to constrain  $H_0$ 

$$P(H_0; M_l | LC) \propto P(H_0) P(M_l)$$

$$\int P(\Delta t_{AB} | M_l; H_0) P(\Delta t_{AB} | LC) d\Delta t_{AB} \qquad (2)$$

where  $P(H_0)$  is a prior probability for  $H_0$ ,  $P(M_l)$  is a prior probability for model l, and  $P(\Delta t_{A,B}|M_l;H_0)$  is the likelihood of  $\Delta t_{A,B}$ , given the model prediction and a value of  $H_0$ .

We include in our likelihood function the relative time delays between four image pairs, S2 and S1, S3 and S1, S4 and S1, and SX and S1, and magnification ratios of three image pairs, S2/S1, S3/S1, and SX/S1 (the exclusion of the magnification ratio S4/S1 is discussed below), and the position of the reappearance. For the set of observables  $\mathcal{O}$ , we find

$$P(H_0|\text{LC}) \propto P(H_0) \sum_{l} P(M_l)$$
 
$$\int P(\mathcal{O}|M_l; H_0) P(\mathcal{O}|\text{LC}) d\mathcal{O}_1 ... d\mathcal{O}_n \qquad (3)$$

Including these observables, in addition to the SX to S1 time delay, allows us to weight each model's contribution to the  $H_0$  inference according to its ability to reproduce the observables (15). We only include observables in the likelihood function if their values were not available to lens modelers before they made their pre-reappearance predictions.

Figure 1 shows the predicted position of the final image (SX) from each lens model, overlaid on a difference image showing the detected position of SX. We use the SX position in the likelihood calculation because it was not

known when the pre-reappearance models were constructed.

The HST F125W and F160W light curves of image S4 have very strong evidence (>5σ) that the SN overlaps a region of high magnification because of one or more stars (or stellar remnants) in the foreground cluster lens (microlensing) (8). The apparent F125W-F160W color of S4 is bluer than the other four images of the SN by  $0.28 \pm 0.05$  mag in the first 150 days after its peak brightness (in the observer frame) and 1.8  $\pm$  0.4 mag after 150 days [figure 12 of (8)]. This bluer color implies that (i) the SN does not have a uniform color and (ii) it overlaps a region, called a caustic, where the magnification due to stars changes abruptly, which causes differential magnification (8). Simulations of lensing of an azimuthally symmetric synthetic SN, with properties similar to those of SN Refsdal (37), by objects in the foreground cluster lens do not predict microlensing events with color differences as large as that observed for S4 [figure 6 of (8)]. Therefore, we exclude the magnification ratio of S4 to S1 because we cannot model accurately the extreme microlensing event, cannot correct its magnification, or assign an uncertainty.

The observables  $\mathcal{O}$  we use to compute likelihoods are a set inferred from the light curve

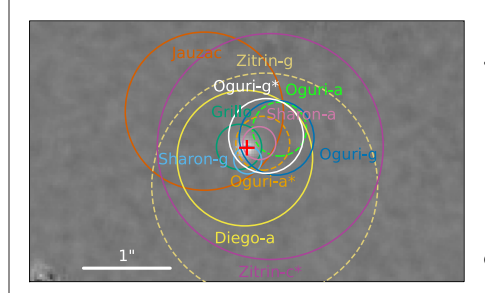


Fig. 1. Comparison between the predicted and actual positions of the reappearance of SN Refsdal image SX in late 2015. Grayscale shows the difference between a coaddition of HST F125W images taken after the appearance of SX (December 2015 through May 2016) and a coaddition of F125W imaging acquired before the reappearance of SX (before July 2015). SX appears as a white source in this presentation. at coordinates listed in table S1. Overlain are colored circles indicating the positions predicted by each model (labeled next to each circle). The radius of each circle indicates the root mean square (RMS) of the offsets between the predicted and observed positions of all multiply imaged galaxies used as constraints on the lens model (29, 30). The pre-reappearance Oguri-a prediction is dashed bright green, and the revised position of the Oguri-a\* model, after including SX's position as a constraint, is dashed light orange. The location of the circle shown for Zitrin-c\* in solid purple was not computed before the reappearance.

$$\mathcal{O}_{1j} = \left[ \Delta t_{2,1}, \Delta t_{3,1}, \Delta t_{4,1}, \Delta t_{\mathrm{X},1}, \mu_2/\mu_1, \mu_3/\mu_1, \mu_\mathrm{X}/\mu_1 \right] \tag{4}$$

where  $\Delta t_{j,1}$  is the relative time delay between the jth image and S1, and  $\mu_i/\mu_1$  is the ratio of the magnifications of image jth and image S1. Two additional observables describe SX's position

$$\mathcal{O}_{\mathbf{p}} = [\alpha_{\mathbf{X}}, \delta_{\mathbf{X}}]$$
 (5)

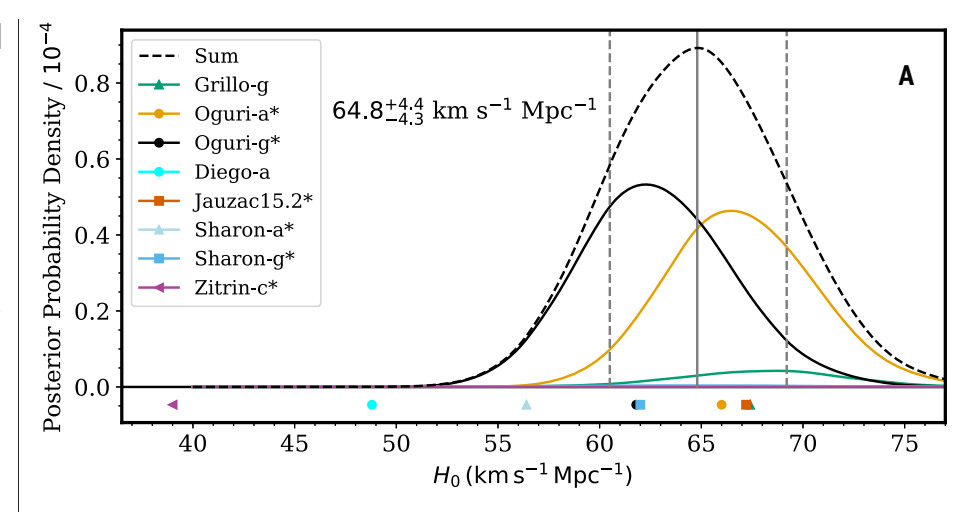
where  $\alpha_X$  and  $\delta_X$  are (respectively) the right ascension and declination coordinates of SX. The measured ratios of the relative time delays of the images, magnification ratios, and relative positions of the images are all independent of  $H_0$ .

## Lens models

Table S2 lists the lens models of MACS J1149 that were published before the appearance of SX: There are eight models from six research groups (29, 30). We use these models, with updates described below, to constrain  $H_0$ . The Bradac and Merten models were not used to make predictions and were excluded from the time-delay calculations (34).

Several of the published pre-reappearance calculations have required revisions. The first Zitrin calculation was amended to address an issue affecting the time-delay surface (29). Although their underlying mass models have remained the same, the Sharon-a, Sharon-g, and Jauzac15.1 time-delay predictions required revisions by ~20% because of technical issues affecting their time-delay calculations (30, 34). The observed location of SX differed by >10 from that predicted by the Oguri-a and Oguri-g models (Fig. 1), so we also updated the Oguri-a and Oguri-g models by adding SX's position as a constraint. To preserve blinding, the direction of the ~1σ shift in the SX to S1 time delay was not disclosed until after we unblinded the time-delay measurement. We use an asterisk to denote models whose predictions were updated or first made after the reappearance. When computing the likelihood of each model, we use pre-reappearance Oguri predictions for SX's position.

For the first of our parallel estimates of  $H_0$ , we use the full set of eight pre-reappearance models, after the corrections above. The Diego-a and Zitrin-c\* models were not able to reproduce the Einstein cross. The second parallel estimate for the value of  $H_0$  uses only the Grillo-g and Oguri-a\* models because their time-delay calculations did not require large corrections (~20%), and they reproduced the positions of the four images S1 to S4 with <0.1" precision. These two models were selected before unblinding the time-delay measurement. With the exception of the Jauzac model, all other model predictions were published as part of an organized effort (29). These models were given the choice to use only the images of



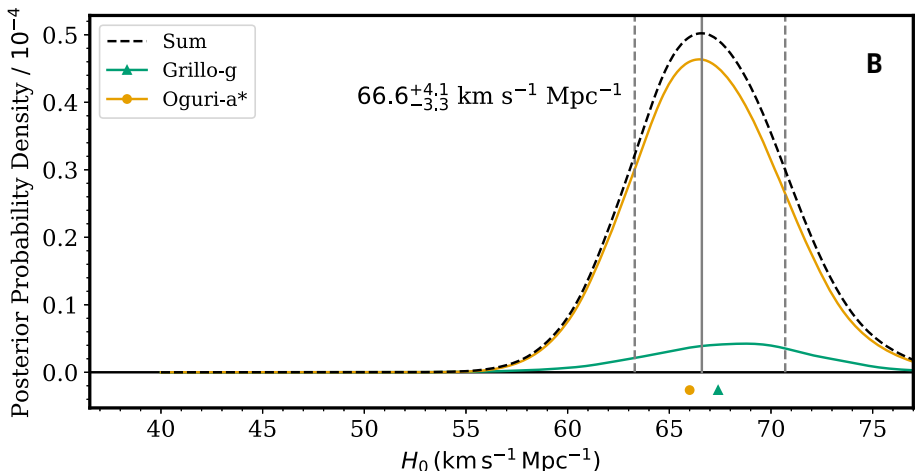


Fig. 2. Constraints on Ho from SN Refsdal. (A) Constraints using the full set of eight models constructed before the reappearance, some with subsequent updates. (B) Parallel constraints using the subset of two pre-appearance models: the Grillo-g and the Oguri-a\* model, with the latter only updated using the reappearance's position. Both panels show the posterior probability densities for each model as colored lines (see legend), and their sum (dashed black line), assuming a uniform prior. The colored markers beneath each plot show the most probable value of H<sub>0</sub> for each of the models, calculated from their predicted SX to S1 time delays. The vertical gray lines show the most likely value from the summed distribution, with the pair of dashed vertical lines marking the 16th and 84th percentile confidence intervals. Models were weighted by their ability to describe the data (Table 2), so for most models in (A), the probability densities are very small with the lines overlapping zero. The purple arrow for Zitrin-c\* in (B) points toward the model's most probable value of  $H_0$ , which is smaller than 39 km s<sup>-1</sup> Mpc<sup>-1</sup>.

Table 1. H<sub>0</sub> constraints and weights determined by posterior probabilities for each set of **lens-model predictions.** The first column lists the most probable value of  $H_0$  and our 16th, 84th, and 99.7th percentile confidence levels. Other columns list the weights (out of 1.0) we calculated using the constraints from SN Refsdal. The first and second rows are our parallel estimates of the value of  $H_0$  using all eight models and our two preferred models, respectively. The relative weights are proportional to the models' posterior probabilities. Dashes indicate not applicable.

(km s <sup>-1</sup> l	Mpc <sup>-1</sup> )								
Confidence	levels	Diego-a	Grillo-g	Jauzac15.2*		Oguri-g*			Zitrin-c*
16-50-84	99.7								
64.8 <sup>+4.4</sup> <sub>-4.3</sub>	73.6	7.1 × 10 <sup>-6</sup>	0.044	$1.0 \times 10^{-5}$	0.44	0.51	0.00072	0.0062	$3 \times 10^{-9}$
66.6+4.1	74.8	_	0.091	_	0.91		_	_	

Weight of each model

 $H_0$ 

strongly lensed galaxies with spectroscopic redshifts (referred to as the gold sample) or all the images of strongly lensed galaxies. We label models using the gold sample with a "g" suffix and those that used all images with an "a" suffix. The Grillo team only produced a model using the gold set of images. The Oguri models were created with both sets, but its authors preferred the Oguri-a\* model over the Oguri-g\* model (28). We therefore chose to adopt the Oguri-a\* model.

Table S2 also lists several models that were produced after the reappearance, which could therefore not make pre-reappearance predictions for SX. For completeness, we also calculated a value of  $H_0$  that includes these models without using SX's position, but we do not regard it as a blinded result.

## Likelihood calculation

We used light-curve simulations to compute the likelihood of the data, given a value of  $H_0$ . In total, 1000 sets of simulated light curves of S1 to SX were produced (8) for random relative magnifications and time delays. These light curves have noise characteristics and measurement cadences that closely approximate the SN Refsdal observations and include the lensing effects of the expected population of darkmatter subhalos and stars in the foreground cluster (8). The simulated light curves are used to measure and correct the bias associated with the four light-curve fitting algorithms (8) and construct a Gaussian mixture model for the likelihood of the observations that accounts for the covariance among the measurements (34).

## H<sub>0</sub> constraints

For the two parallel estimates of  $H_0$ , table S3 lists the values of our unblinded measurements of the relative time delays and magnification ratios, including the companion paper's constraint on the SX to S1 time delay of  $376.0_{-5.5}^{+5.6}$  days (8). Gravitational lensing magnification has a sign (positive or negative) associated with it, but only the absolute value of the magnification can be measured directly through observations of images' brightnesses. When we unblinded the revised Oguri-a\* and Oguri-g\* model predictions, by analyzing Markov chain Monte Carlo (MCMC) chains of lens model parameters, we did not anticipate that the predicted magnification values (which we had not inspected) included the magnification's sign. After unblinding, the

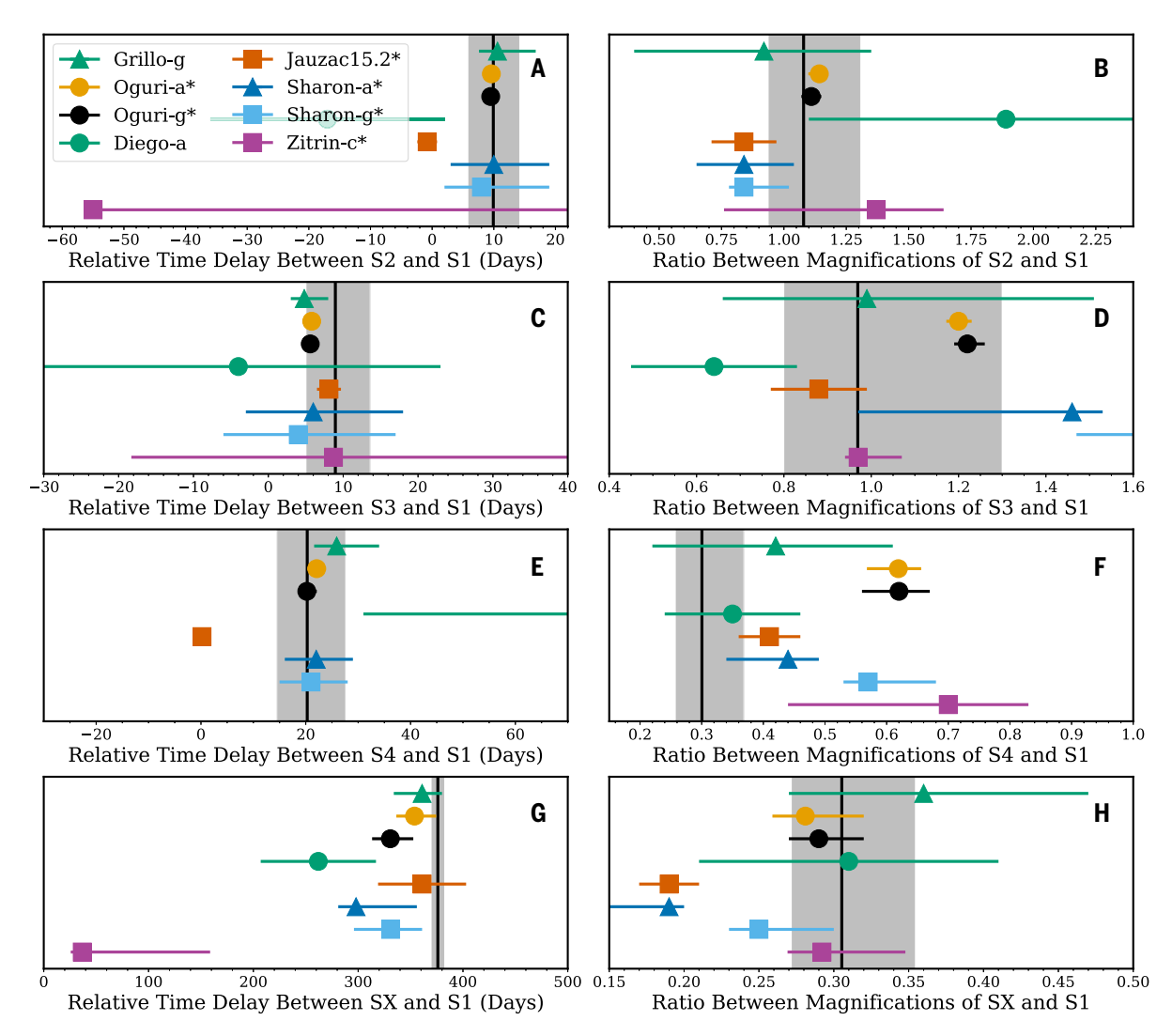


**Fig. 3. Model predictions and measured relative time delays and magnification ratios between images S2 to SX and S1.** (**A**, **C**, **E**, and **G**) Relative time delays between images S2 to SX and S1. (Colored bars indicate the model predictions (see legend), with dots at the median value and bars extending to the 16th and 84th percentiles (8). (**B**, **D**, **F**, and **H**) Same, but for the ratios of the magnification of images S2 to SX and S1. (A) and (B) compare S1 with S2, (C) and (D) compare S1 with S3, (E) and (F) compare S1 with S4, and (G) and (H) compare S1 with SX. Models with an asterisk were revised after SX was observed. The predicted time delays shown were computed for  $H_0 = 70 \text{ km s}^{-1} \text{ Mpc}^{-1}$ .

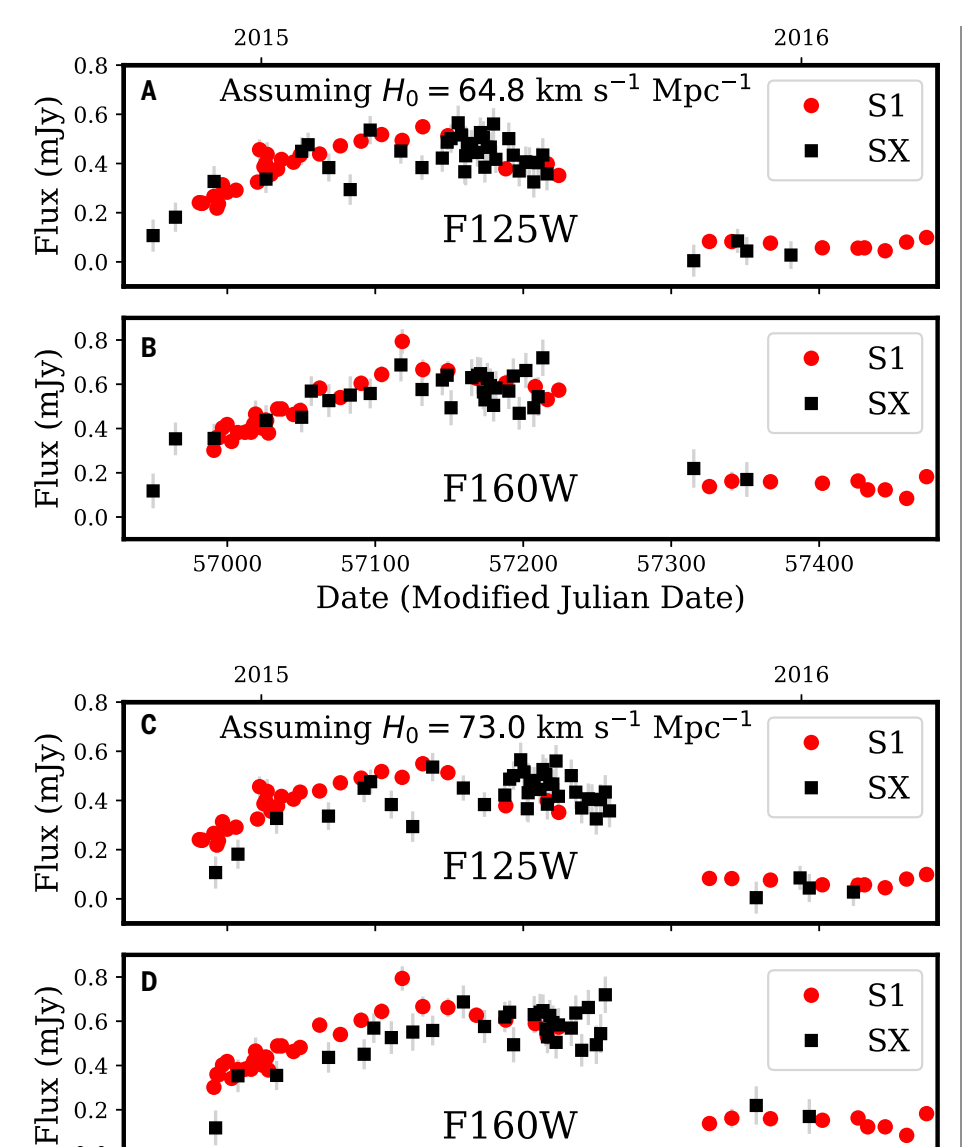


Fig. 4. Shifted light curves of images S1 and SX. (A and B) Fluxes of the images S1 (red circles) and SX (black squares) in the F125W filter (A) and the F160W filter (B), shown as a function of time after removing the measured 376.0-day delay (8), which corresponds to a constraint on the value of  $H_0$ of  $64.8^{+4.4}_{-4.3}$  km s<sup>-1</sup> Mpc<sup>-1</sup>. mJy, millijansky. (**C** and **D**) The same light curves but using the delay of 333.8 days expected for  $H_0 = 73.04 \,\mathrm{km \, s^{-1} \, Mpc^{-1}}$ , the value inferred from the SN distance ladder (10) given the eight pre-reappearance models weighted according to their ability to reproduce the  $H_0$ -independent observables. While we fixed the SX to S1 time delay, we allow the magnification ratio of SX and S1 to vary in our model fitting. The ratios of the magnifications of SX and S1 that minimize the  $\chi^2$  value between a piecewise polynomial model of the light curve (8) and the measured photometry are 0.31 and 0.32, respectively. Error bars show  $1\sigma$  uncertainties. The  $\gamma^2$  difference between the calculations for the two time delays is 58.1 with 178 degrees of freedom, favoring (A) and (B) over (C) and (D).

F160W

57200

Date (Modified Julian Date)

57300

57400

negative magnifications affected the weights of the Oguri-a\* and Oguri-g\* models, but the issue was immediately apparent. We report it for transparency; we addressed it by applying an absolute value function to the magnification used in the weighting pro-

57000

57100

cess. The only other postblinding changes to our analysis were choosing to present an additional estimate of  $H_0$  that includes all pre-reappearance models (not just the preferred models) and to use SX's position instead of the SX to S1 angular separation to weigh models, which changed the results by  $0.1 \text{ km s}^{-1} \text{ Mpc}^{-1}$ .

When we consider all eight pre-reappearance models, we find  $H_0 = 64.8^{+4.4}_{-4.3} \,\mathrm{km \, s^{-1} \, Mpc^{-1}}$ (Fig. 2). The weights for all eight models, listed in Table 1, show that the Oguri-a\* and Oguri-g\* models receive weights of 0.44 and 0.51, respectively, whereas the Grillo-g model receives 0.044 (from a total of 1.0). Figure 3, A to H, shows a comparison between the constraints on the observables and the model predictions. The Oguri models are the best match to the observations, which is why they received higher weights. When we consider only the Grillo-g and Oguri-a\* models, we find  $H_0 =$  $66.6^{+4.1}_{-3.3}$  km s<sup>-1</sup> Mpc<sup>-1</sup>. In this sample, Grillo-g receives a weight of 0.091, and Oguri-a\* receives a weight of 0.91. For all models listed in table S2 that can be used to make time-delay calculations, even those produced after the appearance of SX, we find  $H_0 = 64.6^{+4.4}_{-4.2} \, \mathrm{km \ s}^{-1}$  $\mathrm{Mpc}^{-1}$  (fig. S3). The latter calculation does not use the position of SX to weight models because it was already known when some of those models were produced.

The measured value of the delay is  $376.0^{+5.6}_{-5.5}$  days (8), which yields  $H_0 = 64.8^{+4.4}_{-4.3}$  km s<sup>-1</sup> Mpc<sup>-1</sup> considering the eight pre-reappearance models. We next calculate the time delay expected if  $H_0$  is equal to the value found by the SH0ES local distance ladder. For  $H_0 =$  $73.04 \, \mathrm{km} \, \mathrm{s}^{-1} \, \mathrm{Mpc}^{-1}$ , the weighted combination of the eight pre-reappearance models yields a delay between SX and S1 of 333.8 days.

While holding the time delay between SX and S1 fixed but allowing the ratio of their magnifications to vary, we fitted the F125W and F160W light curves of SX and S1 using a piecewise polynomial model (8). This model describes the light curve in each filter as two polynomials. The first, a third order polynomial, applies before 150 days after peak brightness, and the second, a second-order polynomial, applies at later epochs. We first fix the SX to S1 time delay to 333.8 days (corresponding to  $H_0=73~{\rm km~s^{-1}\,Mpc^{-1}})$  and then to 376.0 days  $(H_0=64.8^{+4.4}_{-4.3}~{\rm km~s^{-1}\,Mpc^{-1}})$ . The fixed 333.8-day SX to S1 delay yields a worse  $\chi^2$  greater by 58.1 for 178 degrees of freedom. We conclude that a shorter time delay of 333.8 days for  $H_0 = 73 \text{ km s}^{-1} \text{ Mpc}^{-1}$  and a flexible model provide a substantially worse match to the observations of SN Refsdal. Figure 4 shows the light curves of images S1 and SX shifted by 376.0 days (Fig. 4, A and B) and 333.8 days (Fig. 4, C and D). The ratios of the magnifications of SX and S1 that minimize the  $\chi^2$  value between a piecewise polynomial model of the light curve (8) and the measured photometry are 0.31 and 0.32, respectively.

Figure 5A compares our measurements of  $H_0$  from SN Refsdal with previous results using both the late-time and early-time Universe constraints. The posterior probability

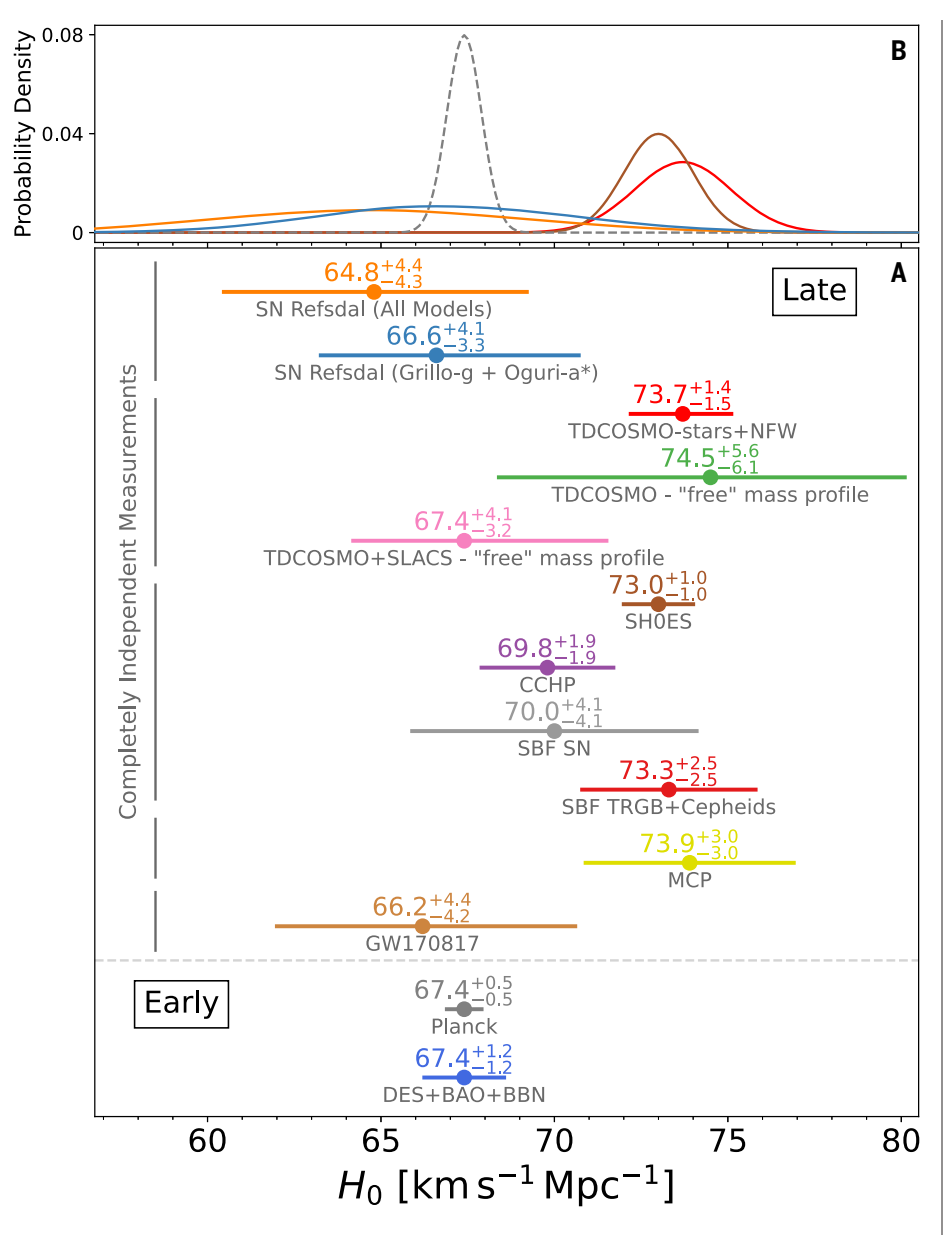


**Fig. 5. Comparison of the** *H*<sub>0</sub> **measurement using SN Refsdal with previous measurements.** (**A**) Constraints from our measurements of SN Refsdal for the full set of eight models (orange) and our preferred subset of the two best models (blue). These are compared with previous constraints from SH0ES + Gaia (*10*), the Carnegie-Chicago Hubble Program (CCHP) (*12*), H0 Lenses in COSMOGRAIL's Wellspring (H0LICOW) (*13*), STRong lensing Insight into DES (STRIDES) (*40*), surface brightness fluctuations (SBF) SN (*41*), SBF Tip of the Red Giant Branch (TRGB)+Cepheids (*42*), Megamaser Cosmology Project (MCP) (*43*), gravitational wave event GW 170817 (*44*), Planck (*9*), and Dark Energy Survey (DES) + Baryon Acoustic Oscillation (BAO) + Big Bang nucleosynthesis (BBN) (*45*). (**B**) posterior probability densities for SN Refsdal (orange and blue), Planck [*(9)*, dashed gray], SH0ES (*10*), and H0LICOW (*13*). Error bars show the 16th, 50th, and 84th percentile confidence levels. Dashed horizontal line separates measurements from observations of the early Universe from the late Universe. *H*<sub>0</sub> measurements bracketed by different vertical gray bars are entirely independent of each other. Figure generated using a previous comparison (*46*).

Table 2. Posterior probability for each set of lens-model predictions.												
Diego-a	Grillo-g	Jauzac15.2*	Oguri-g*	Oguri-a*	Sharon-a*	Sharon-g*	Zitrin-c*					
$7 \times 10^{-9}$	$4.3 \times 10^{-5}$	9.9 × 10 <sup>-9</sup>	0.00043	0.0005	$7.1 \times 10^{-7}$	$6.1 \times 10^{-6}$	$3 \times 10^{-12}$					

distributions from our  $H_0$  measurement are shown in Fig. 5B along with several previous measurements of the expansion rate. Our two estimates of  $H_0$  using SN Refsdal favor values for  $H_0$  that are smaller than the SH0ES estimate (10) by 8.2 km s<sup>-1</sup> Mpc<sup>-1</sup> and 6.4 km s<sup>-1</sup> Mpc<sup>-1</sup>, which correspond to 1.8 $\sigma$  and 1.5 $\sigma$ , respectively. Our most probable values of  $H_0$  are smaller by 2.6 km s<sup>-1</sup> Mpc<sup>-1</sup> and 0.8 km s<sup>-1</sup> Mpc<sup>-1</sup>, corresponding to differences of 0.6 $\sigma$  and 0.2 $\sigma$ , respectively, from the value of  $H_0$  inferred from early-Universe observations (9).

## Systematic uncertainties and error budget

We considered two sets of models for our parallel estimates of  $H_0$ , but every model separately prefers smaller values of  $H_0$  than 68 km s<sup>-1</sup> Mpc<sup>-1</sup> given the SX to S1 time delay (Fig. 2). We check whether our measurement of  $H_0$  is robust to the assumptions of the simply parameterized models using a model produced after the appearance of SX. The Chen2020 model (38) makes only minimal assumptions about the distribution of matter at the cluster scale; it calculates an SX to S1 time delay of 332.35  $\pm$ 9.32 days assuming  $H_0 = 70 \, \mathrm{km \, s^{-1}}$  Mpc<sup>-1</sup> (38), consistent with those of the simply parameterized models (table S4). The Chen2020 model also reproduces the Einstein cross.

The closely related Oguri-a\* and Oguri-g\* models account for 95% of the weight for our primary estimate of  $H_0$ , whereas the Oguri-a\* model accounts for 91% of the weight of our parallel estimate (Table 1). Given the model's weights, we use the MCMC chain for the Oguri-a\* model to construct an error budget for the model. We split the Oguri-a\* model parameters (28) into six sets of related parameters and construct a second-order model of the predicted SX to S1 time delay in terms of these variables, after subtracting the mean value of each parameter from the values of the parameters (34). We next compute the reduction in the variance of the predicted SX to S1 time delay when we add each group of model parameters in succession.

There is covariance among the groups of model parameters, so we compute the mean of the reduction of the variance after repeating the calculation for all permutations of the groups of parameters. The resulting error budget (fig. S4) shows that the cluster's principal dark-matter halo, which dominates its mass, has the largest contribution to the uncertainty in  $H_0$ .

We used the Hera galaxy cluster simulation (33) to assess the ability of the Oguri models to recover the value of  $H_0$  by applying the same modeling code [Glafic (28, 39)] to the simulation. In fig. S5, we compare the time delays and uncertainties estimated from the Hera simulation (33) with those estimated using the Glafic code. This comparison assumes the same cosmological parameters that were

used to construct the Hera simulations ( $H_0=72~{\rm km~s^{-1}~Mpc^{-1}}$  and  $\Omega_M=0.24$ ). We find that the recovered and actual time delays in fig. S5 are correlated, with a best-fitting slope of  $1.046\pm0.021$ . We infer that GLAFIC can be used to infer  $H_0$  within ~5%, consistent with the error budget calculated for SN Refsdal.

Both the Grillo and Oguri teams performed their time-delay calculations using the positions of images S1 and SX as predicted by their models. We examined whether the models' SX to S1 time delays would shift if the images' observed positions instead are used (34); we find differences of <2 days (table S4), less than the precision of the measured time delay. An independent investigation by the Grillo team into the accuracy of  $H_0$  estimated using SN Refsdal found that a 3% constraint on the relative S1 to SX time delay corresponds to 6% uncertainty in  $H_0$  (17), which is consistent with our uncertainty calculations.

## Analytical expectation for H<sub>0</sub> uncertainty

The change in  $H_0$  due to an overprediction or underprediction of the separation of two images of a strongly lensed object can be described by a simple differential equation (35). We use this relationship, and the predicted image positions for S1 and SX in the MCMC chain for the Oguri-a\* model, to compute the expected uncertainty in  $H_0$ . We find that the precision with which the Oguri-a\* model reproduces the separation of SX and S1 corresponds to a 5.5% uncertainty in  $H_0$ . We also find that ~92% of the variance in the relative time delay of SX and S1 can be accounted for by the predicted separation of the two images. Therefore, we conclude that our ~5% error budget for the Oguri-a\* model is consistent with the analytic expectation.

## SN cosmography with a cluster lens

We have used observations of SN Refsdal to perform cosmography and measure the cosmic expansion rate. Using two sets of models, we derived constraints on  $H_0$  of  $64.8^{+4.4}_{-4.3} \, \mathrm{km \, s^{-1}}$  Mpc<sup>-1</sup> and  $66.6^{+4.1}_{-3.3} \, \mathrm{km \, s^{-1}}$  Mpc<sup>-1</sup>.

We expect that our results have different systematic uncertainties compared with other methods for measuring  $H_0$ , including time-delay cosmography using quasars, which instead use galaxy-scale lenses. The dominant source of uncertainty in our  $H_0$  measurement is the cluster lens model. The 1.5% uncertainty in the measurement of the SX to S1 time delay (8) is sufficiently small that it would provide an equally precise constraint on the value of  $H_0$  if the cluster model were perfect.

Our analysis uses lens models that were blind to the time-delay measurement. The models that account for almost all of the weight in our estimate of  $H_0$  are consistent with the observations (Fig. 3), with the exception of

the relative magnification of image S4, which appears to have experienced a microlensing event. The simply parameterized models best reproduce the observables, even when the CMB and SN constraints on  $H_0$  are used as priors (see supplementary text). We analyzed our error budget using the Oguri-a\* model, finding that our ~5.5% uncertainty on  $H_0$  is consistent with analytic expectations (35) given the model's astrometric accuracy. Further tests using a simulated galaxy cluster also indicated an expected uncertainty of ~5%.

#### **REFERENCES AND NOTES**

- S. Refsdal, On the Possibility of Determining Hubble's Parameter and the Masses of Galaxies from the Gravitational Lens Effect. Mon. Not. R. Astron. Soc. 128, 307–310 (1964). doi: 10.1093/mnras/128.4.307
- T. Treu, P. J. Marshall, Time delay cosmography. Astron. Astrophys. Rev. 24, 11 (2016). doi: 10.1007/s00159-016-0096-8
- M. Tewes et al., COSMOGRAIL: The COSmological Monitoring of GRAvItational Lenses. Astron. Astrophys. 556, A22 (2013). doi: 10.1051/0004-6361/201220352
- S. H. Suyu et al., Cosmology from gravitational lens time delays and Planck data. Astrophys. J. Lett. 788, L35 (2014). doi: 10.1088/2041-8205/788/2/L35
- S. Birrer et al., TDCOSMO IV. Hierarchical time-delay cosmography – joint inference of the Hubble constant and galaxy density profiles. Astron. Astrophys. 643, A165 (2020). doi: 10.1051/0004-6361/202038861
- P. L. Kelly et al., Multiple images of a highly magnified supernova formed by an early-type cluster galaxy lens. Science 347, 1123–1126 (2015). doi: 10.1126/science.aaa3350; pmid: 25745167
- P. L. Kelly et al., Deja vu all over again: The reappearance of supernova Refsdal. Astrophys. J. Lett. 819, L8 (2016). doi: 10.3847/2041-8205/819/1/L8
- P. L. Kelly et al., The Magnificent Five Images of Supernova Refsdal: Time Delay and Magnification Measurements. Astrophys. J. 948, 93 (2023). doi: 10.3847/1538-4357/ac4ccb
- Planck Collaboration, Planck 2018 results VI. Cosmological parameters. Astron. Astrophys. 641, A6 (2020). doi: 10.1051/ 0004-6361/201833910
- A. G. Riess et al., A Comprehensive Measurement of the Local Value of the Hubble Constant with 1 km s<sup>-1</sup> Mpc<sup>-1</sup> Uncertainty from the Hubble Space Telescope and the SH0ES Team. Astrophys. J. Lett. 934, L7 (2022). doi: 10.3847/ 2041-8213/ac5c5b
- L. Verde, T. Treu, A. G. Riess, Tensions between the early and late Universe. *Nat. Astron.* 3, 891–895 (2019). doi: 10.1038/ s41550-019-0902-0
- W. L. Freedman et al., The Carnegie-Chicago Hubble Program.
   VIII. An Independent Determination of the Hubble Constant Based on the Tip of the Red Giant Branch. Astrophys. J. 882, 34 (2019). doi: 10.3847/1538-4357/ab2f73
- M. Millon et al., TDCOSMO I. An exploration of systematic uncertainties in the inference of H<sub>0</sub> from time-delay cosmography. Astron. Astrophys. 639, A101 (2020). doi: 10.1051/0004-6361/201937351
- S. Birrer et al., HOLiCOW IX. Cosmographic analysis of the doubly imaged quasar SDSS 1206+4332 and a new measurement of the Hubble constant. Mon. Not. R. Astron. Soc. 484, 4726–4753 (2019). doi: 10.1093/mnras/stz200
- J. Vega-Ferrero, J. M. Diego, V. Miranda, G. M. Bernstein, The Hubble Constant from SN Refsdal. Astrophys. J. Lett. 853, L31 (2018). doi: 10.3847/2041-8213/aaa95f
- C. Grillo et al., Measuring the Value of the Hubble Constant "à la Refsdal." Astrophys. J. 860, 94 (2018). doi: 10.3847/ 1538-4357/aac2c9
- C. Grillo et al., On the Accuracy of Time-delay Cosmography in the Frontier Fields Cluster MACS JI149.5+2223 with Supernova Refsdal. Astrophys. J. 898, 87 (2020). doi: 10.3847/ 1538-4357/ab9a4c
- M. Oguri, Strong gravitational lensing of explosive transients. *Rep. Prog. Phys.* 82, 126901 (2019). doi: 10.1088/1361-6633/ ab4fc5; pmid: 31634885
- M. Oguri, Y. Kawano, Gravitational lens time delays for distant supernovae: Breaking the degeneracy between radial mass profiles and the Hubble constant. *Mon. Not. R. Astron. Soc.* 338, L25–L29 (2003). doi: 10.1046/j.1365-8711.2003.06290.x

- G. Dobler, C. R. Keeton, Microlensing of Lensed Supernovae. Astrophys. J. 653, 1391–1399 (2006). doi: 10.1086/508769
- A. Goobar et al., iPTF16geu: A multiply imaged, gravitationally lensed type la supernova. Science 356, 291–295 (2017). doi: 10.1126/science.aal2729; pmid: 28428419
- X. Li, J. Hjorth, J. Richard, The rates and time-delay distribution of multiply imaged supernovae behind lensing clusters. J. Cosmol. Astropart. Phys. 2012, 015 (2012). doi: 10.1088/1475-7516/2012/11/015
- A. von der Linden et al., Weighing the Giants I. Weak-lensing masses for 51 massive galaxy clusters: Project overview, data analysis methods and cluster images. Mon. Not. R. Astron. Soc. 439, 2–27 (2014). doi: 10.1093/mnras/stt1945
- P. L. Kelly et al., Weighing the Giants II. Improved calibration of photometry from stellar colours and accurate photometric redshifts. Mon. Not. R. Astron. Soc. 439, 28–47 (2014). doi: 10.1093/mnras/stt1946
- D. E. Applegate et al., Weighing the Giants III. Methods and measurements of accurate galaxy cluster weak-lensing masses. Mon. Not. R. Astron. Soc. 439, 48–72 (2014). doi: 10.1093/mnras/stt/21/9
- H. Ebeling, A. C. Edge, J. P. Henry, MACS: A Quest for the Most Massive Galaxy Clusters in the Universe. Astrophys. J. 553, 668–676 (2001). doi: 10.1086/320958
- A. Zitrin, T. Broadhurst, Discovery of the largest known lensed images formed by a critically convergent lensing cluster. Astrophys. J. 703, L132–L136 (2009). doi: 10.1088/0004-637X/703/2/L132
- R. Kawamata, M. Oguri, M. Ishigaki, K. Shimasaku, M. Ouchi, Precise strong lensing mass modeling of four *Hubble* Frontier Field clusters and a sample of magnified high-redshift galaxies. *Astrophys. J.* 819, 114 (2016). doi: 10.3847/ 0004-637X/819/2/114
- T. Treu et al., "Refsdal" meets Popper: Comparing predictions of the re-appearance of the multiply images supernova behind MACSJ1149.5+2223. Astrophys. J. 817, 60 (2016). doi: 10.3847/0004-637X/817/1/60
- M. Jauzac et al., Hubble Frontier Fields: Predictions for the return of SN Refsdal with the MUSE and GMOS spectrographs. Mon. Not. R. Astron. Soc. 457, 2029–2042 (2016). doi: 10.1093/mnras/stw069
- P. L. Kelly et al., Detection of a SN near the center of the galaxy cluster field MACS1149 consistent with predictions of a new image of Supernova Refsdal. Astron. Telegr. 8402, 1 (2015).
- S. A. Rodney et al., SN Refsdal: Photometry and time delay measurements of the first Einstein Cross supernova. Astrophys. J. 820, 50 (2016). doi: 10.3847/0004-637X/820/1/50
- M. Meneghetti et al., The Frontier Fields lens modelling comparison project. Mon. Not. R. Astron. Soc. 472, 3177–3216 (2017). doi: 10.1093/mnras/stx2064
- Materials and methods are available as supplementary materials.
- S. Birrer, T. Treu, Astrometric requirements for strong lensing time-delay cosmography. Mon. Not. R. Astron. Soc. 489, 2097–2103 (2019). doi: 10.1093/mnras/stz2254
- P. L. Kelly et al., Hubble Space Telescope Discovery of a Probable Caustic-Crossing Event in the MACS1149 Galaxy Cluster Field. Astron. Telegr. 9097, 1 (2016).
- L. Dessart, D. J. Hillier, Supernovae from blue supergiant progenitors: What a mess! Astron. Astrophys. 622, A70 (2019). doi: 10.1051/0004-6361/201833966
- W. Chen, P. L. Kelly, L. L. R. Williams, Blind Prediction of the Returning Image of Supernova Refsdal from a New Lens Model of the Galaxy Cluster MACS J1149.5+2223. Res. Notes AAS 4, 215 (2020). doi: 10.3847/2515-5172/abcf2b
- M. Oguri, The Mass Distribution of SDSS J1004 + 4112 Revisited. *Publ. Astron. Soc. Jpn.* 62, 1017–1024 (2010). doi: 10.1093/pasj/62.4.1017
- A. J. Shajib et al., STRIDES: A 3.9 per cent measurement of the Hubble constant from the strong lens system DES J0408 –5354. Mon. Not. R. Astron. Soc. 494, 6072–6102 (2020). doi: 10.1093/mnras/staa828
- N. Khetan et al., A new measurement of the Hubble constant using Type la supernovae calibrated with surface brightness fluctuations. Astron. Astrophys. 647, A72 (2021). doi: 10.1051/ 0004-6361/202039196
- J. P. Blakeslee, J. B. Jensen, C.-P. Ma, P. A. Milne, J. E. Greene, The Hubble Constant from Infrared Surface Brightness Fluctuation Distances. Astrophys. J. 911, 65 (2021). doi: 10.3847/1538-4357/abe86a
- D. W. Pesce et al., The Megamaser Cosmology Project. XIII. Combined Hubble Constant Constraints. Astrophys. J. Lett. 891, L1 (2020). doi: 10.3847/2041-8213/ab75f0

- T. Dietrich et al., Multimessenger constraints on the neutronstar equation of state and the Hubble constant. Science 370, 1450–1453 (2020). doi: 10.1126/science.abb4317; pmid: 33335061
- T. M. C. Abbott et al., Dark Energy Survey Year 1 Results: A Precise H<sub>0</sub> Estimate from DES Y1, BAO, and D/H Data. Mon. Not. R. Astron. Soc. 480, 3879–3888 (2018). doi: 10.1093/ mnras/sty1939
- V. Bonvin, M. Millon, HOLiCOW HO tension plotting notebook, v1.0, Zenodo (2020); https://doi.org/10.5281/zenodo.3635517.
- P. Kelly, Constraints on the Hubble constant for Supernova Refsdal's reappearance, Zenodo (2023); https://doi.org/ 10.5281/zenodo.7818787.

#### **ACKNOWLEDGMENTS**

We thank program coordinators B. Periello and T. Royle as well as contact scientists N. Pirzkal, I. Momcheva, and K. Sahu of the Space Telescope Science Institute (STScI) for their help carrying out the HST observations. We also appreciate useful discussions with P. Rosati, C. Grillo, S. Suyu, and M. Meneghetti. We used the HFF Lens Model website, hosted by the Mikulski Archive for Space Telescopes (MAST) at STScI. Funding: P.L.K., A.V.F., T.T., J.P., and S.R. received financial support from NASA/STScI grants GO-14041, 14199, 14208, 14528, 14872, 14922, 15050, 15791, and 16134. P.L.K. is supported by NSF grant AST-1908823. M.O. acknowledges support by the WPI Initiative (MEXT, Japan) and by JSPS KAKENHI grants JP18K03693, JP20H00181, JP20H05856, and JP22H01260. T.T. acknowledges the support of NSF grant AST-1906976. S.T. was supported by the Cambridge Centre for Doctoral Training in Data-Intensive Science funded by the UK

Science and Technology Facilities Council (STFC). J.P. was supported by the NASA FINESST award 80NSSC19K1414. J.M.D. acknowledges the support of project PGC2018-101814-B-100 (MCIU/AEI/MINECO/FEDER, UE) Ministerio de Ciencia, Investigación y Universidades. J.M.D. was funded by the Agencia Estatal de Investigación, Unidad de Excelencia María de Maeztu, ref. no. MDM-2017-0765. M.J. is supported by the United Kingdom Research and Innovation (UKRI) Future Leaders Fellowship (grant MR/S017216/1). M.M. and V.B. acknowledge support from the European Research Council (ERC) under the Horizon 2020 Research and Innovation Program (COSMICLENS: grant agreement 787886). A.V.F. is grateful for funding from the Christopher R. Redlich Fund, the TABASGO Foundation, the UC Berkeley Miller Institute for Basic Research in Science (as a Miller Senior Fellow), and financial contributions from many additional individual donors. R.J.F. is supported in part by NASA grant NNG17PX03C, NSF grants AST-1518052 and AST-1815935, the Gordon and Betty Moore Foundation, the Heising-Simons Foundation, and the David and Lucile Packard Foundation. J.H. acknowledges support from VILLUM FONDEN investigator grant 16599. S.J. is supported by NSF CAREER award AST-0847157 as well as by NASA/Keck JPL RSA 1508337 and 1520634, K.M. acknowledges funding from the European Union's Horizon 2020 Research and Innovation Program under ERC grant agreement no. 101002652 and Marie Skłodowska-Curie grant agreement no. 873089. A.Z. acknowledges support by grant no. 2020750 from the United States-Israel Binational Science Foundation (BSF), by grant no. 2109066 from the US NSF, and by the Ministry of Science and Technology, Israel. Author contributions: P.L.K. measured the SN photometry, developed the statistical framework and analysis

code, and drafted the manuscript. P.L.K., S.R., T.T., A.V.F., R.J.F., J.H., T.B., O.G., S.J., C.M., M.P., K.B.S., B.E.T., and A.v.d.L. obtained follow-up HST imaging. P.L.K., S.R., T.T., S.B., V.B., L.D., D.G., K.M., M.M., J.P., K.S., and S.T. contributed to the time-delay measurement. P.L.K., S.R., T.T., V.B., A.V.F., K.M., and S.T. helped prepare the manuscript. S.R., T.T., L.W., T.B., and A.D. aided the interpretation. M.O., W.C., A.Z., J.M.D., and M.J. modeled the galaxy cluster. Competing interests: The authors declare no competing interests. Data and materials availability: The HST imaging is available from https://mast.stsci.edu/ search/ui/#/hst under proposal IDs 14041, 14199, 14208, 14528, 14872, and 14922. The measured time delays and magnifications are listed in table S3, and the predicted values are listed in tables S4 and S5. Our analysis code is archived on Zenodo (47). License information: Copyright © 2023 the authors, some rights reserved; exclusive licensee American Association for the Advancement of Science. No claim to original US government works. https://www.science.org/about/science-licenses-journal-article-reuse

#### SUPPLEMENTARY MATERIALS

science.org/doi/10.1126/science.abh1322 Materials and Methods Supplementary Text Figs. S1 to S6

Figs. S1 to S6
Tables S1 to S15
References (48–67)

Submitted 22 February 2021; accepted 24 April 2023 Published online 11 May 2023 10.1126/science.abh1322



## Constraints on the Hubble constant from supernova Refsdal's reappearance

Patrick L. Kelly, Steven Rodney, Tommaso Treu, Masamune Oguri, Wenlei Chen, Adi Zitrin, Simon Birrer, Vivien Bonvin, Luc Dessart, Jose M. Diego, Alexei V. Filippenko, Ryan J. Foley, Daniel Gilman, Jens Hjorth, Mathilde Jauzac, Kaisey Mandel, Martin Millon, Justin Pierel, Keren Sharon, Stephen Thorp, Liliya Williams, Tom Broadhurst, Alan Dressler, Or Graur, Saurabh Jha, Curtis McCully, Marc Postman, Kasper Borello Schmidt, Brad E. Tucker, and Anja von der Linden

Science 380 (6649), eabh1322. DOI: 10.1126/science.abh1322

## **Editor's summary**

The Hubble constant measures the expansion rate of the Universe, but different methods give inconsistent values. Kelly *et al.* studied a supernova that had its light split into multiple images by the gravitational lensing of a foreground galaxy cluster. They combined measurements of the time delay between the multiple images with predictions made by multiple lensing models of the cluster. This approach allowed the authors to make a blinded measurement of the Hubble constant, finding a value that is more consistent with that derived from the cosmic microwave background than with the cosmic distance ladder. —Keith T. Smith

## View the article online

https://www.science.org/doi/10.1126/science.abh1322

## **Permissions**

https://www.science.org/help/reprints-and-permissions

Use of this article is subject to the Terms of service